Polarization observables in low-energy antiproton-proton scattering

Daren Zhou and Rob G. E. Timmermans

KVI, Theory Group, University of Groningen, Zernikelaan 25, NL-9747 AA Groningen, The Netherlands

We investigate the polarization parameters in low-energy antiproton-proton elastic ($\overline{p}p \rightarrow \overline{p}p$) and charge-exchange ($\overline{p}p \rightarrow \overline{n}n$) scattering. The predictions for unmeasured observables are based on our new energy-dependent partial-wave analysis of all antiproton-proton scattering data below 925 MeV/c antiproton laboratory momentum, which gives an optimal description of the existing database. Sizable and remarkable spin effects are observed, in particular for charge-exchange scattering. These result from the spin dependence of the long- and medium-range one- and two-pion exchange antinucleon-nucleon potential and the state dependence of the parametrized short-range interaction. We study the possibility of polarizing a circulating antiproton beam with a polarized proton target by exploiting the spin dependence of the $\overline{p}p$ total cross section. It appears feasible to achieve a significant transverse polarization of an antiproton beam within a reasonable time.

I. INTRODUCTION

The invention of stochastic cooling by van der Meer made it possible to accumulate antiprotons in a high-quality beam [1]. As a result, the antinucleon-nucleon ($\overline{N}N$) interaction could be studied at the Low Energy Antiproton Ring (LEAR) at CERN. Experimental data of good quality could be obtained down to antiproton momenta of about 200 MeV/c. The observables measured were mostly differential cross sections for antiproton-proton elastic ($\overline{p}p \rightarrow \overline{p}p$) and charge-exchange ($\overline{p}p \rightarrow \overline{n}n$) scattering. With a polarized proton target the analyzing power for elastic [2–5] and charge-exchange [6–9] scattering was measured for a number of antiproton momenta, and initial data for the depolarization parameter in elastic [10] and charge-exchange [11,12] scattering and for the spin-transfer parameter in charge-exchange [13] scattering were acquired. It has always been a dream of the antiproton physics community to have available a high-quality polarized antiproton beam. In recent years, definite plans have been proposed for a physics program with polarized antiprotons, for instance by the collaboration for Polarized Antiproton eXperiments (PAX) [14,15]. Experiments with a polarized antiproton beam and a polarized proton target would give full access to the complicated spin dependence of the $\overline{N}N$ interaction and could help to unveil the spin structure of the (anti)proton and test predictions of nonperturbative QCD.

In this article, we present theoretical predictions for spin observables in $\overline{p}p$ elastic and charge-exchange scattering. Our results are based on the recent new energy-dependent partial-wave analysis (PWA) [16] that we performed of all $\overline{p}p$ scattering data below 925 MeV/c. The method of PWA was originally developed for pp and np scattering [17–23] and enabled major steps forward for the field of few-nucleon physics [24,25]. It was adapted to $\overline{p}p \rightarrow \overline{p}p, \overline{n}n$ scattering in Refs. [26–28] and to the hyperon production reactions $\overline{p}p \rightarrow \overline{Y}Y$ in Refs. [29–32]. The PWA exploits as much as possible our knowledge of the long-range interaction to describe the energy dependence of the (spin-dependent) scattering amplitude, while the unknown short-range interaction that gives only slow energy variations to the amplitudes is parametrized phenomenologically. In this way, a model-independent and high-quality description of the scattering data is realized, and the predictive power for thus-far unmeasured observables is optimal [28].

In Ref. [16] the long-range part of the strong $\overline{p}p$ interaction is described by the one-pion and two-pion exchange interactions derived from the effective chiral Lagrangian of QCD. Notable features are a strong central attraction in the elastic $\overline{p}p \rightarrow \overline{p}p$ channel and a strong tensor force, in particular for charge-exchange $\overline{p}p \rightarrow \overline{n}n$ scattering. The short-range part of the interaction, including the coupling of the $\overline{p}p, \overline{n}n$ system to the mesonic annihilation channels, is parametrized by a complex, energy-dependent boundary condition at $r = 1.2$ fm. The PWA describes the existing $\overline{p}p$ database, which contains 3749 scattering data with an excellent $\chi^2_{\min}/N_{\mathrm{df}} = 1.048$, where $N_{\mathrm{df}} = 3578$ is the number of degrees of freedom.

The organization of our paper is as follows: In Sec. II we explore the various polarization observables in elastic and charge-exchange scattering and the predictions of the PWA. We exhibit some sizable spin effects that could, for instance, be exploited experimentally to produce polarized antineutrons. Our study is similar in spirit to that of Ref. [33], in which spin observables were discussed qualitatively before LEAR came into operation by using a simple optical-potential model. In Sec. III, we discuss how to exploit the spin dependence of the $\overline{p}p$ interaction to polarize a low-energy antiproton beam. We summarize in Sec. IV.

II. SPIN OBERVABLES

The scattering formalism that we use is standard (see for instance Refs. [34–39]). Because the strong and electromagnetic interactions obey the discrete symmetries charge-conjugation, parity, and time-reversal invariance, the $\overline{N}N$ scattering observables can be calculated as a function of the scattering angle in the center-of-mass system in terms of five (for the elastic case) or six (for the charge-exchange case) independent

scattering amplitudes $\langle s'm'|M(\theta)|s\,m\rangle$, where s and s' denote the total initial and final spin, respectively, and m and m' are the corresponding z components. Neither for $\overline{N}N$ nor for the better known NN case are enough independent experimental quantities available to determine for a fixed energy these five (or six) amplitudes for every angle θ [40–42]. Therefore, so-called amplitude analyses are not feasible and energy-dependent partial-wave analyses are the tool of choice [28].

We denote a general scattering observable by X_{srbt}, where the indices denote the spin direction of the particles: $s =$ scattered, $r =$ recoil, $b =$ beam, and $t =$ target. It is convenient to use two different coordinate systems for the spin directions: (i) the vectors $\hat{x}$, $\hat{y}$, and $\hat{z}$ define a right-handed coordinate system wherein $\hat{z}$ is the direction of the incoming beam and $\hat{y}$ is normal to the scattering plane; (ii) the spin directions $\hat{l}$, $\hat{m}$, and $\hat{n}$ are tied to the outgoing particles, where $l = p_i + p_f$ and $m = p_f - p_i$ lie in the scattering plane and $\hat{n} = \hat{l} \times \hat{m} = \hat{y}$, and p_i and p_f are the initial and final momenta in the center-of-mass system.

The scattering observables can be expressed in terms of the scattering amplitude as

$$I_0\,X_{srbt} = \tfrac{1}{4}\mathrm{Tr}[\sigma_{1s}\sigma_{2r}M\sigma_{1b}\sigma_{2t}M^\dagger], \qquad (1)$$

where $I_0 = d\sigma/d\Omega = \mathrm{Tr}[MM^\dagger]/4$ is the differential cross section averaged over the spins of the initial-state particles and summed over the spins of the final-state particles ($X_{0000} \equiv 1$). The indices take the values 0, x, y, and z or 0, l, m, and n; $\vec{\sigma}_{1,2}$ are the Pauli spin matrices, and $(\sigma_{1,2})_0$ is the identity matrix used in case of an unpolarized particle or unobserved spin direction. The simplest spin observable is the analyzing power $A_n = A_{000n}$, defined by

$$I_0\,A_n = \tfrac{1}{4}\mathrm{Tr}[M\sigma_{2n}M^\dagger] \qquad (2)$$

(where we replaced X by the conventional symbol A), the measurement of which requires only a polarized proton target. Differential cross sections and analyzing powers of good quality were measured at LEAR for both elastic and charge-exchange scattering.

In order to measure all possible spin observables one needs a polarized proton target, a polarized antiproton beam, and "analyzers" of the polarization of the recoil proton (or neutron) and the scattered antiproton (or antineutron). While there are standard techniques to polarize a proton target, a high-intensity polarized antiproton beam does not exist yet. The polarization of the recoil proton can be measured by secondary scattering on a carbon target. However, carbon is not a good analyzer for the polarization of antiprotons [43] and a proton target gives only about 10% analyzing power for antiprotons. For these reasons, next to the analyzing power A_n, the depolarization $D = D_{0n0n}$ is the easiest spin observable to measure. It was measured, with limited statistical precision, at LEAR for both elastic and charge-exchange scattering for a few antiproton momenta. For charge-exchange scattering also the spin transfer $D_t = K_{n00n}$ was measured. D and D_t are examples of depolarization and spin-transfer observables, defined in general by

$$I_0\,D_{ij} = \tfrac{1}{4}\mathrm{Tr}[\sigma_{2i}M\sigma_{2j}M^\dagger], \qquad (3a)$$

$$I_0\,K_{ij} = \tfrac{1}{4}\mathrm{Tr}[\sigma_{1i}M\sigma_{2j}M^\dagger], \qquad (3b)$$

where $D_{ij} = D_{0i0j}$ for depolarizations and $K_{ij} = K_{i00j}$ for spin transfers. We also define the spin-correlation observables

$$I_0\,C_{ij} = \tfrac{1}{4}\mathrm{Tr}[\sigma_{1i}\sigma_{2j}MM^\dagger], \qquad (4a)$$

$$I_0\,A_{ij} = \tfrac{1}{4}\mathrm{Tr}[M\sigma_{1i}\sigma_{2j}M^\dagger], \qquad (4b)$$

where $C_{ij} = C_{ij00}$ and $A_{ij} = A_{00ij}$.

In a similar way, one can define higher-rank spin observables. In this paper, however, we focus on the above observables, since even these rank-two spin observables are difficult to measure. We point out that sometimes other notations are used in the literature, for instance $A_y = A_{000n}$, $D_{yy} = D_{0n0n}$, and $K_{yy} = K_{n00n}$, etc. Actually, it is often convenient to mix the notations l, m, n and x, y, z. For instance, we can define $R_t = K_{lx}$, $R'_t = K_{mx}$, $A_t = K_{\bar{l}\bar{z}}$, and $A'_t = K_{\bar{m}\bar{z}}$, where the bar means that the spin of the particle points in the opposite direction of the index.

In order to calculate the spin observables, we use as input the scattering amplitudes as predicted by our PWA. As discussed in detail in Refs. [16,27], they contain the Coulomb, magnetic-moment, and nuclear (hadronic) scattering amplitudes. The spin-independent Coulomb amplitude for $\overline{p}p$ elastic scattering is given by

$$\langle s'm'|M_C(\theta)|s\,m\rangle = -\delta_{ss'}\delta_{mm'}\,\frac{\eta}{2p}\,\frac{e^{2i\xi_0}}{\left(\sin^2\tfrac{1}{2}\theta\right)^{1+i\eta}}, \qquad (5)$$

where $\eta = -\alpha/v_{\mathrm{lab}}$ is the relativistic Rutherford parameter, with α the fine-structure constant and v_{lab} the velocity of the incoming antiproton in the laboratory frame; p is its center-of-mass momentum; and $\xi_0 = \arg\Gamma(1 + i\eta)$ is the Coulomb phase shift for orbital angular momentum $\ell = 0$. The magnetic-moment interaction is treated in the Coulomb-distorted-wave Born approximation. It contains a spin-orbit and a tensor force. The main effect is due to the spin-orbit force, which for $\overline{p}p$ elastic scattering results in the spin-dependent amplitude

$$\langle 1\,1|M^C_{C+MM}(\theta)|1\,0\rangle = -\frac{e^{2i\xi_0}}{\sin\theta\sqrt{2}}\,\frac{(8\mu_p - 2)\alpha}{4M_p}$$
$$\times \left[e^{-i\eta\ln\frac{1}{2}(1-\cos\theta)} - \frac{1}{2}(1-\cos\theta)\right]$$
$$= -\langle 1\,0|M^C_{C+MM}(\theta)|1\,1\rangle, \qquad (6)$$

where M_p is the mass of the proton and μ_p its magnetic moment. In practice, η in the square brackets of Eq. (6) is set to zero; the difference from the case when η is nonzero is very small. The nuclear elastic and charge-exchange amplitudes are given by

$$\langle s'm'|M^C_{C+N}(\theta)|s\,m\rangle$$
$$= \sum_{\ell\ell'J}\sqrt{4\pi(2\ell+1)}\,i^{\ell-\ell'}\,C^{\ell\;s\;J}_{0\;m\;m}\,C^{\ell'\;s'\;J}_{m-m'\;m'\;m}\,Y^{\ell'}_{m-m'}(\theta)$$
$$\times\langle\ell's'|S_C^{1/2}\big(S^C_{C+N}-1\big)S_C^{1/2}|\ell\,s\rangle/(2ip), \qquad (7)$$

where the C's are Clebsch-Gordan coefficients, Y is a spherical harmonic, and $|\ell' - \ell| = 0$, 2. S^C_{C+N} is the nuclear S matrix in the presence of the Coulomb force, i.e., matched outside the range of the nuclear forces to Coulomb wave functions. We use
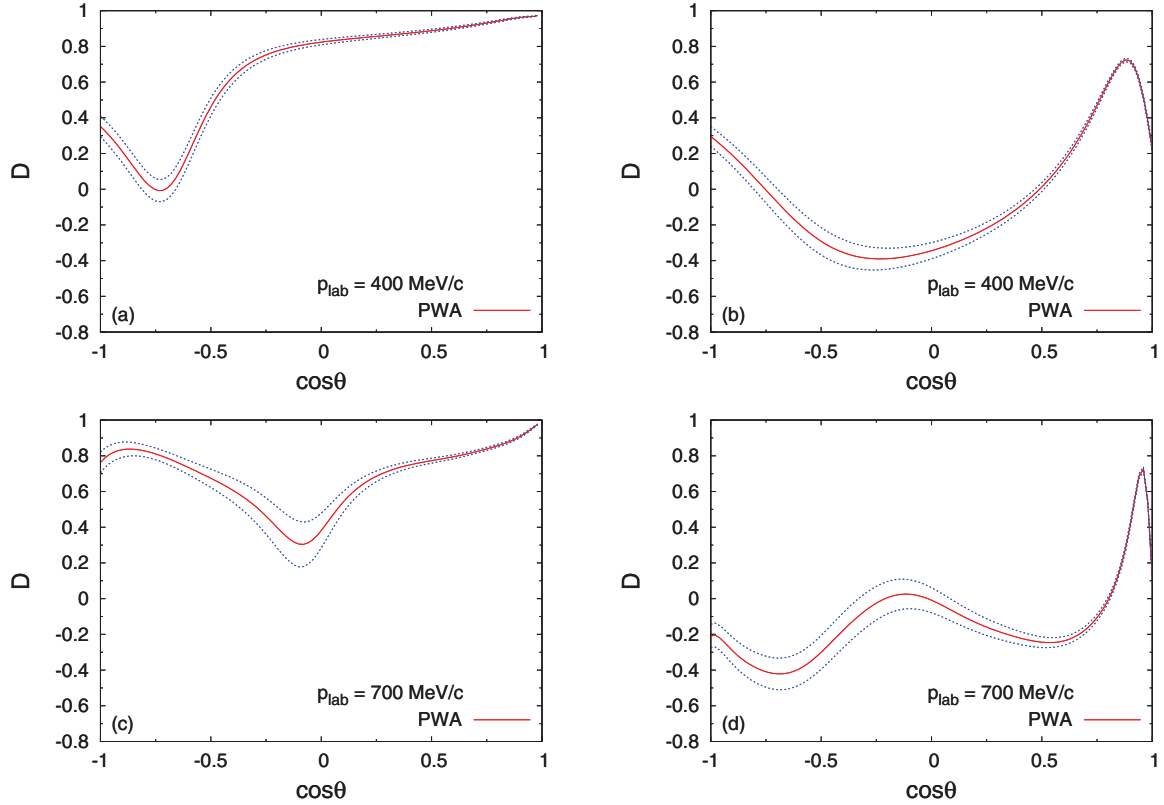
FIG. 1. (Color online) The depolarization D for $\bar{p}p$ elastic (left) and charge-exchange (right) scattering at 400 and 700 MeV/c laboratory momentum. The PWA result is given by the solid red line and the dotted blue lines indicate the 1σ uncertainty region.

matrix notation because of the presence of a tensor force which couples the partial waves with $|\ell' - \ell| = 2$. S_C is the Coulomb S matrix, which is diagonal in spin and orbital angular momentum, with entries $\langle \ell's'|S_C|\ell s\rangle = \delta_{\ell\ell'}\delta_{ss'}\exp(2i\xi_\ell)$, where $\xi_\ell = \arg\Gamma(\ell + 1 + i\eta)$ for elastic scattering. S_C is equal to the identity matrix for charge-exchange scattering.

In Figs. 1–12, we plot the predictions of the PWA [16] for the spin observables D, D_t, R, R', R_t, R'_t, A, A', A_t, A'_t, C_{nn}, and A_{zz} for both elastic and charge-exchange scattering at two typical laboratory momenta $p_{\text{lab}} = 400$ and 700 MeV/c. In all cases, the solid (red) line is the PWA prediction and the two dashed (blue) lines border the one-standard-deviation theoretical uncertainty region. Our results for these observables at other momenta, or predictions for other, higher-rank spin observables, can be calculated straightforwardly and are available upon request. We discuss some of the salient features that are apparent from the results plotted in Figs. 1–12.

In Figs. 1–3 we show the results for the depolarization $D = D_{0n0n}$, the polarization transfer $D_t = K_{n00n}$, and the rotation parameter $R = D_{0m0x}$. The depolarization D for elastic scattering is close to the value 1 for forward angles, especially for low momenta. In the charge-exchange case, D rises rapidly for very forward angles, after which it decreases to negative values for larger angles. The rise for the forward angles is due to one-pion exchange. For elastic scattering, the spin rotation R approaches the value 1 for forward angles.

In Figs. 4–6 we show the results for the rotation parameter $R' = D_{0\ell0x}$ and the polarization transfers $R_t = K_{\ell00x}$ and

$R'_t = K_{m00x}$. For the charge-exchange case, the value of the spin transfer R'_t is large for the very forward angles, especially at low momenta, which implies that the outgoing antineutron is strongly polarized. It may be interesting to study whether it is feasible to produce a polarized antineutron beam in this way.

In Figs. 7–9 we show the results for the rotation parameters $A = D_{0\bar{m}0\bar{z}}$ and $A' = D_{0\bar{\ell}0\bar{z}}$ and the polarization transfer $A_t = K_{\bar{\ell}00\bar{z}}$. The spin rotation A' is large and positive for forward angles for the elastic case, while for the charge-exchange case it is large and negative. For charge-exchange scattering, the spin transfer A_t is forward peaked (due to one-pion exchange), especially at low momenta, resulting in strongly polarized antineutrons. This characteristic could again be exploited to produce a polarized antineutron beam [33].

In Figs. 10–12 we show the results for the polarization transfer $A'_t = K_{\bar{m}0\bar{z}}$ and the spin correlations $C_{nn} = C_{nn00}$ and $A_{zz} = A_{00zz}$. For the charge-exchange case, the spin correlations C_{nn} and A_{zz} vary strongly as a function of angle and reach large values, both positive and negative. A measurement of C_{ij} for the elastic or charge-exchange reactions requires secondary scattering of both the recoil nucleon and the scattering antinucleon. In the strangeness-exchange reactions $\bar{p}p \to \bar{Y}Y$ the "self-analyzing" weak decays of the (anti)hyperons give access to the spin correlations C_{ij} by measuring the angular distributions of the decay products [44–47]. A measurement of A_{zz} requires a polarized antiproton beam and a polarized proton target.
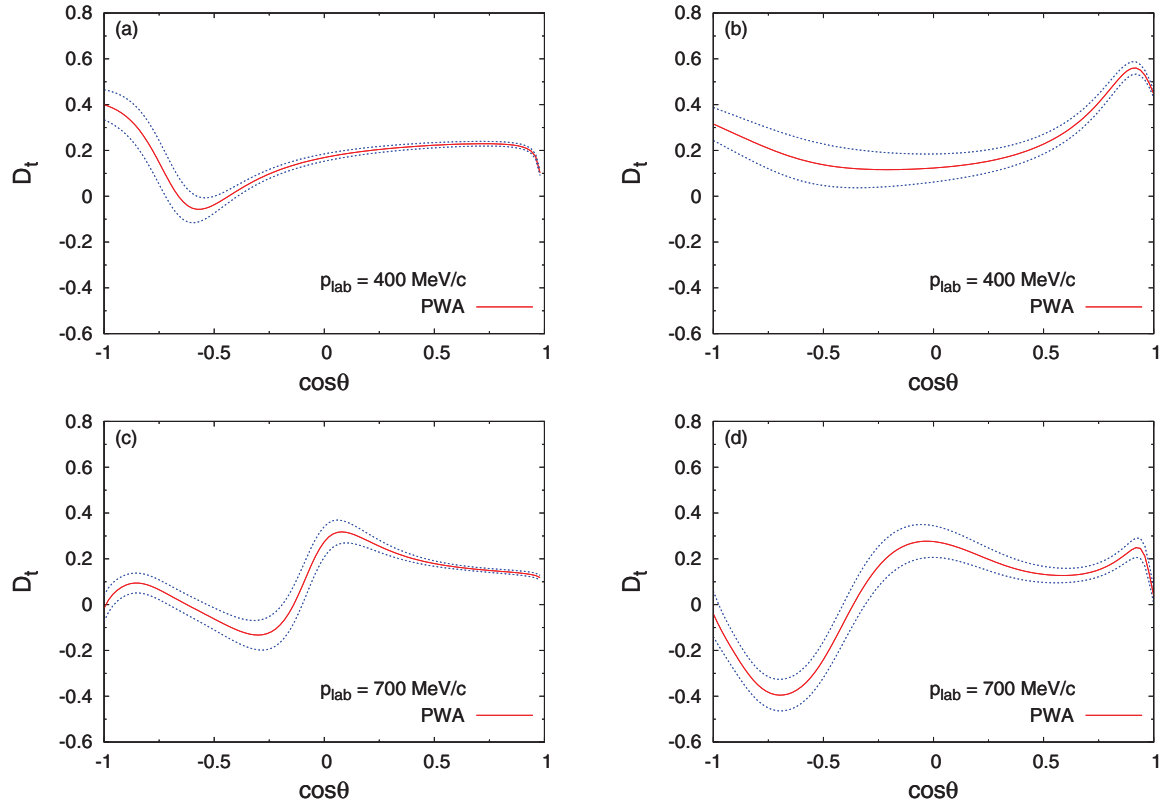
FIG. 2. (Color online) The polarization transfer D_t for $\bar{p}p$ elastic (left) and charge-exchange (right) scattering at 400 and 700 MeV/c laboratory momentum. The PWA result is given by the solid red line and the dotted blue lines indicate the 1σ uncertainty region.
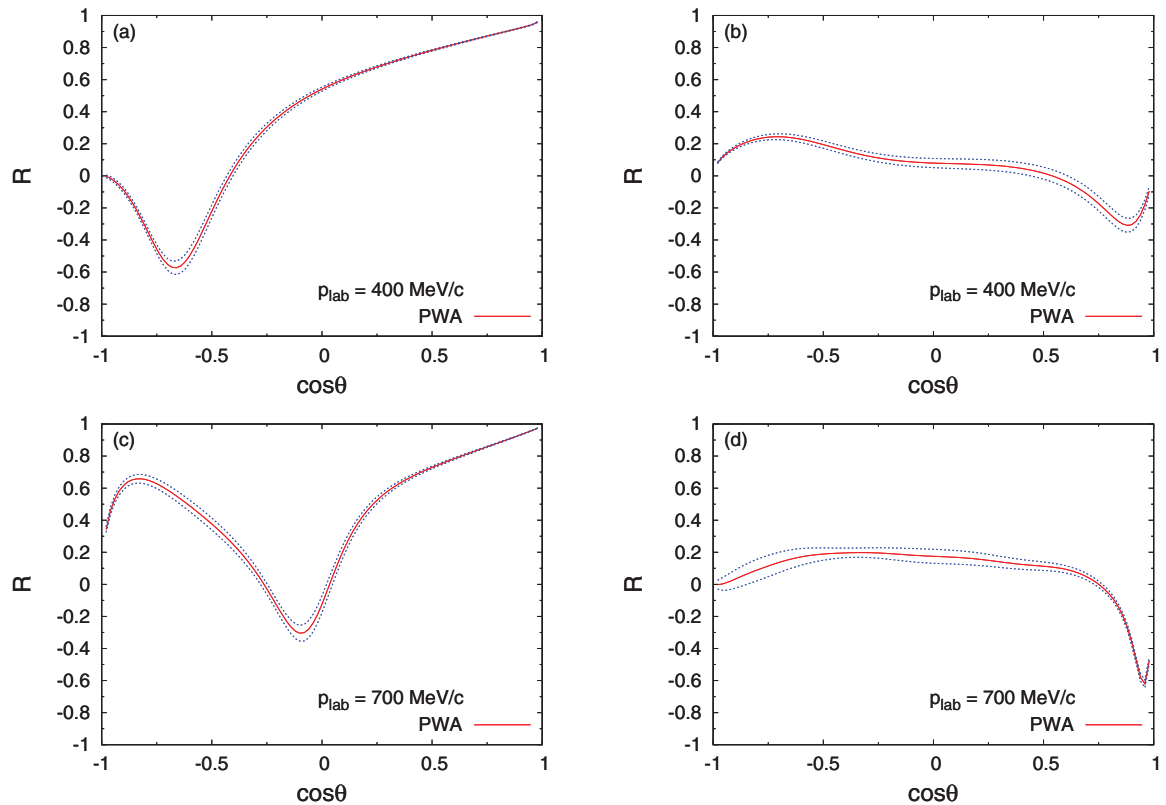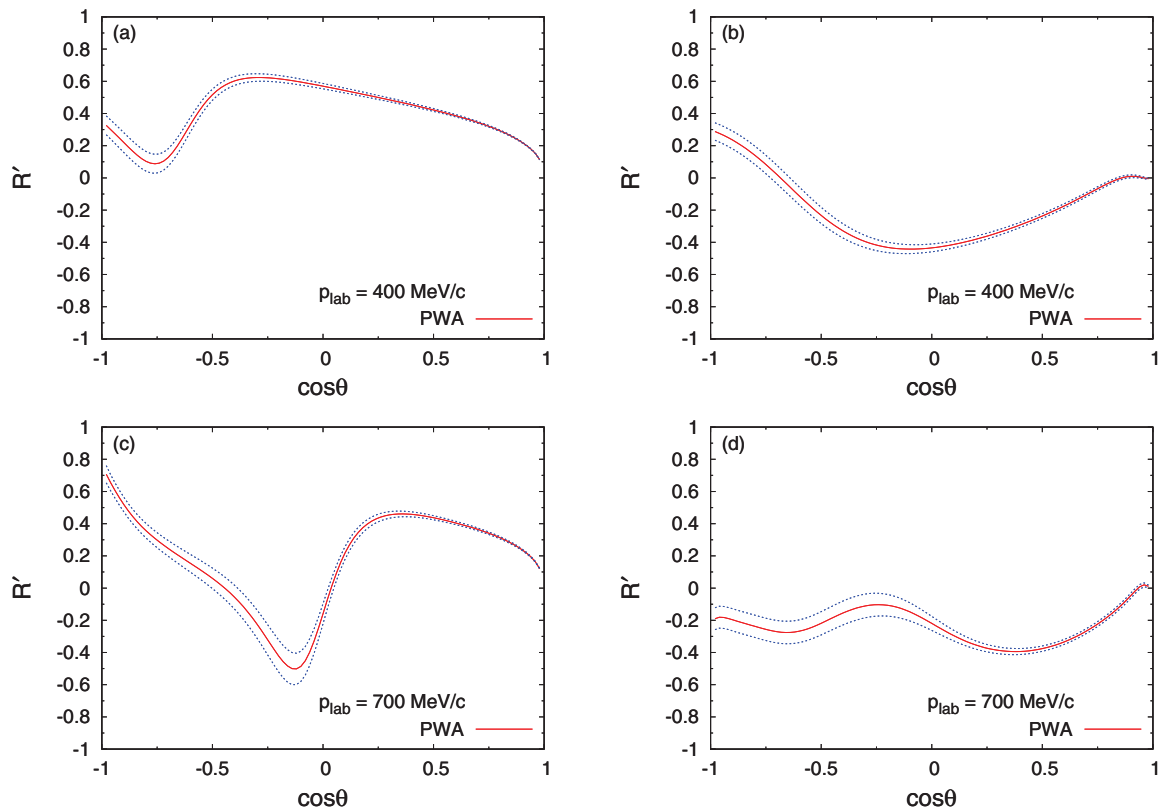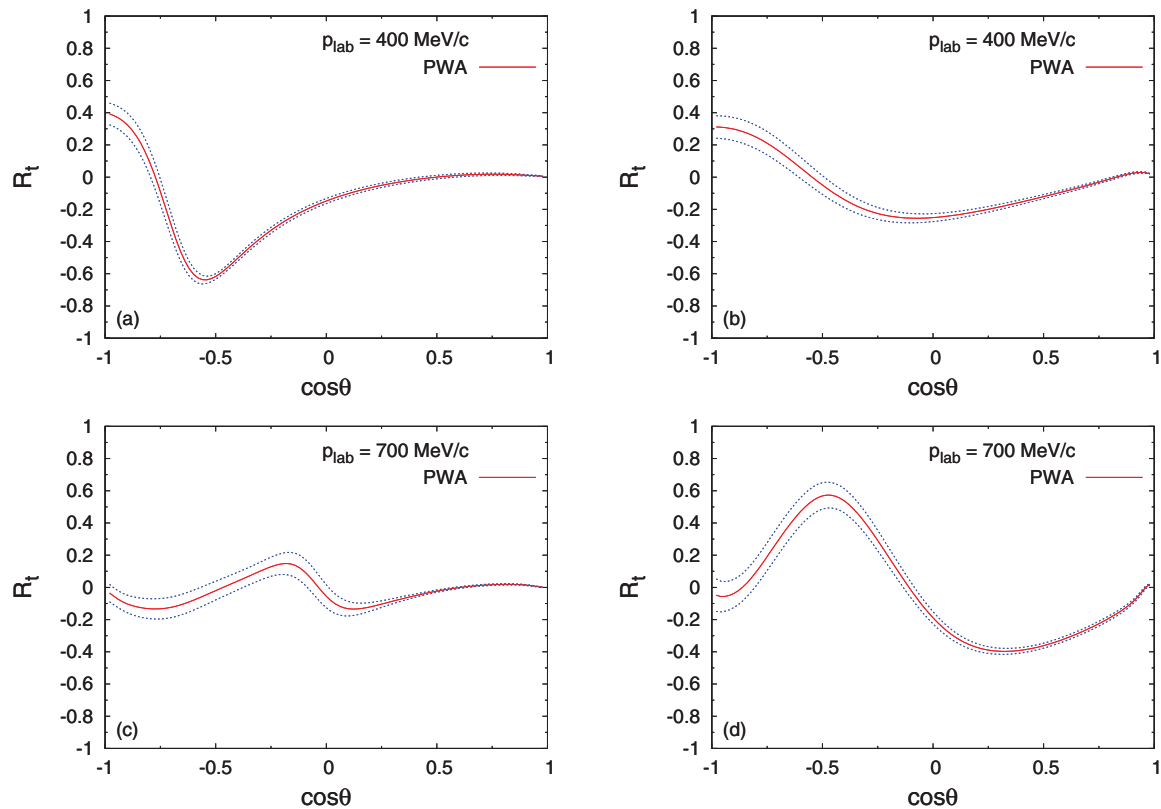

FIG. 3. (Color online) The rotation parameter R for $\bar{p}p$ elastic (left) and charge-exchange (right) scattering at 400 and 700 MeV/c laboratory momentum. The PWA result is given by the solid red line and the dotted blue lines indicate the 1σ uncertainty region.

FIG. 4. (Color online) The rotation parameter R' for $\bar{p}p$ elastic (left) and charge-exchange (right) scattering at 400 and 700 MeV/c laboratory momentum. The PWA result is given by the solid red line and the dotted blue lines indicate the 1σ uncertainty region.
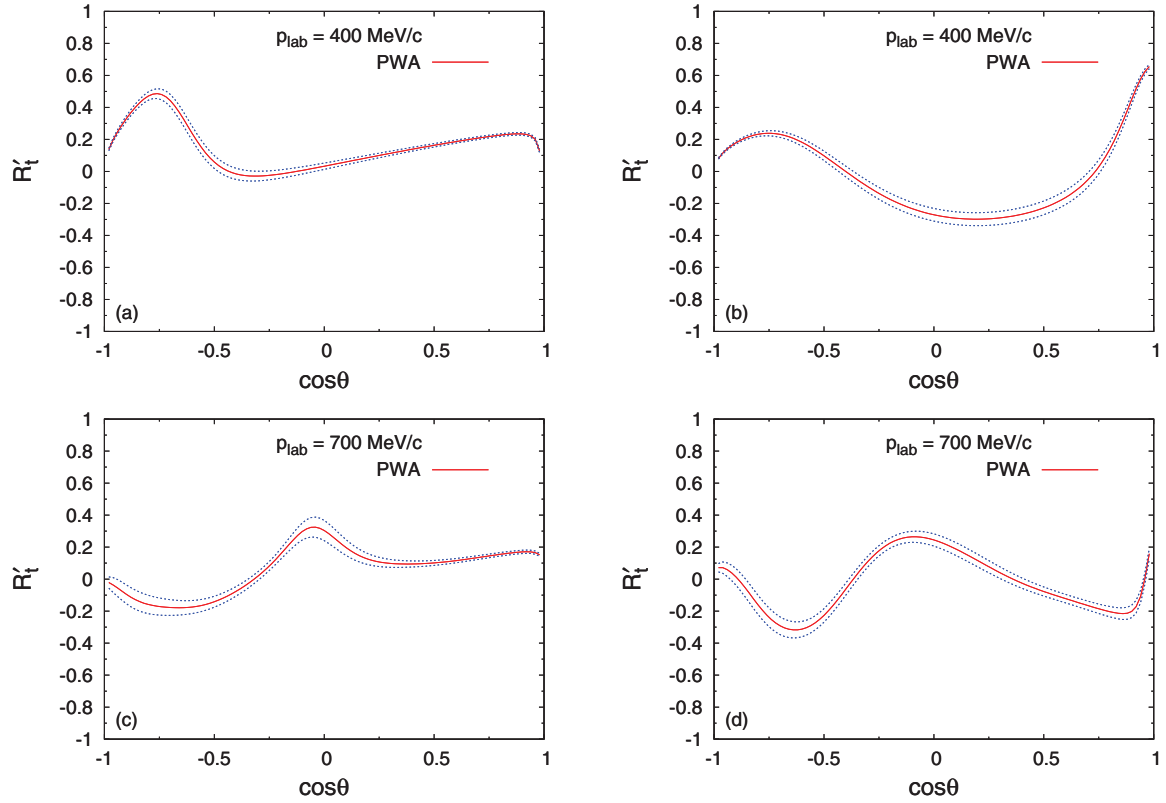

FIG. 5. (Color online) The polarization transfer R_t for $\bar{p}p$ elastic (left) and charge-exchange (right) scattering at 400 and 700 MeV/c laboratory momentum. The PWA result is given by the solid red line and the dotted blue lines indicate the 1σ uncertainty region.

FIG. 6. (Color online) The polarization transfer R'_t for $\bar{p}p$ elastic (left) and charge-exchange (right) scattering at 400 and 700 MeV/c laboratory momentum. The PWA result is given by the solid red line and the dotted blue lines indicate the 1σ uncertainty region.
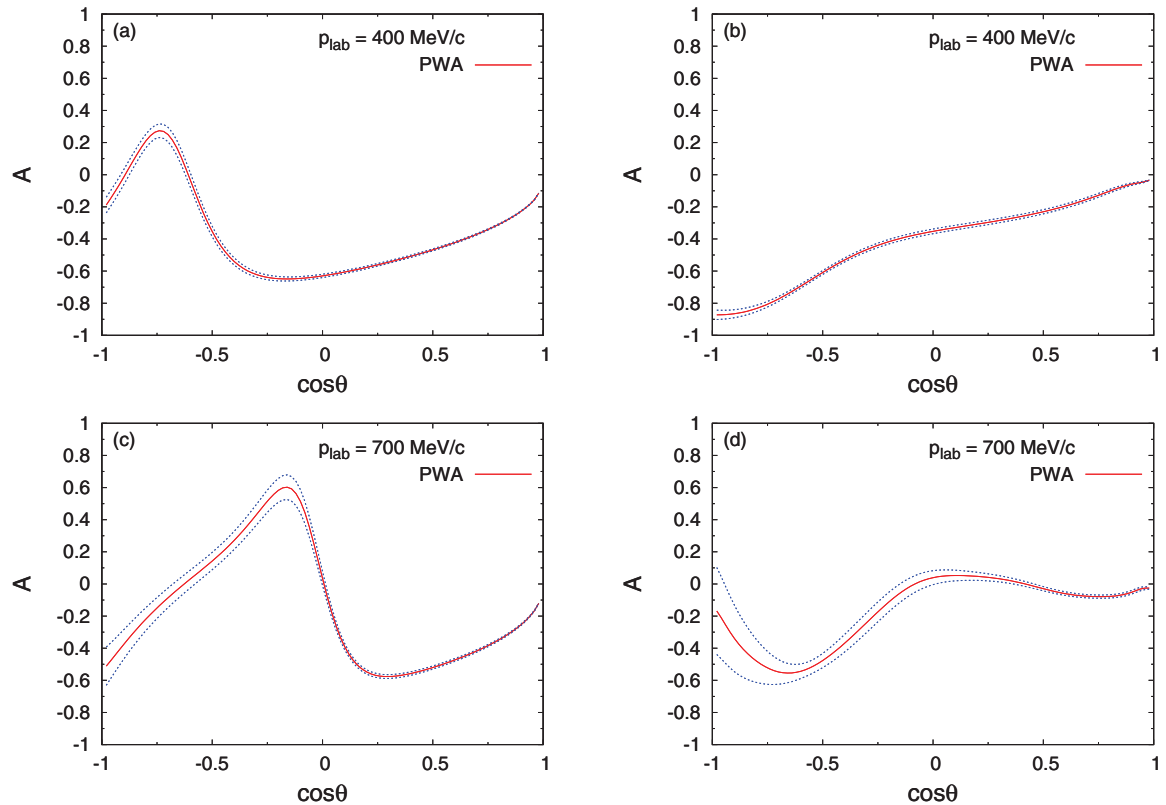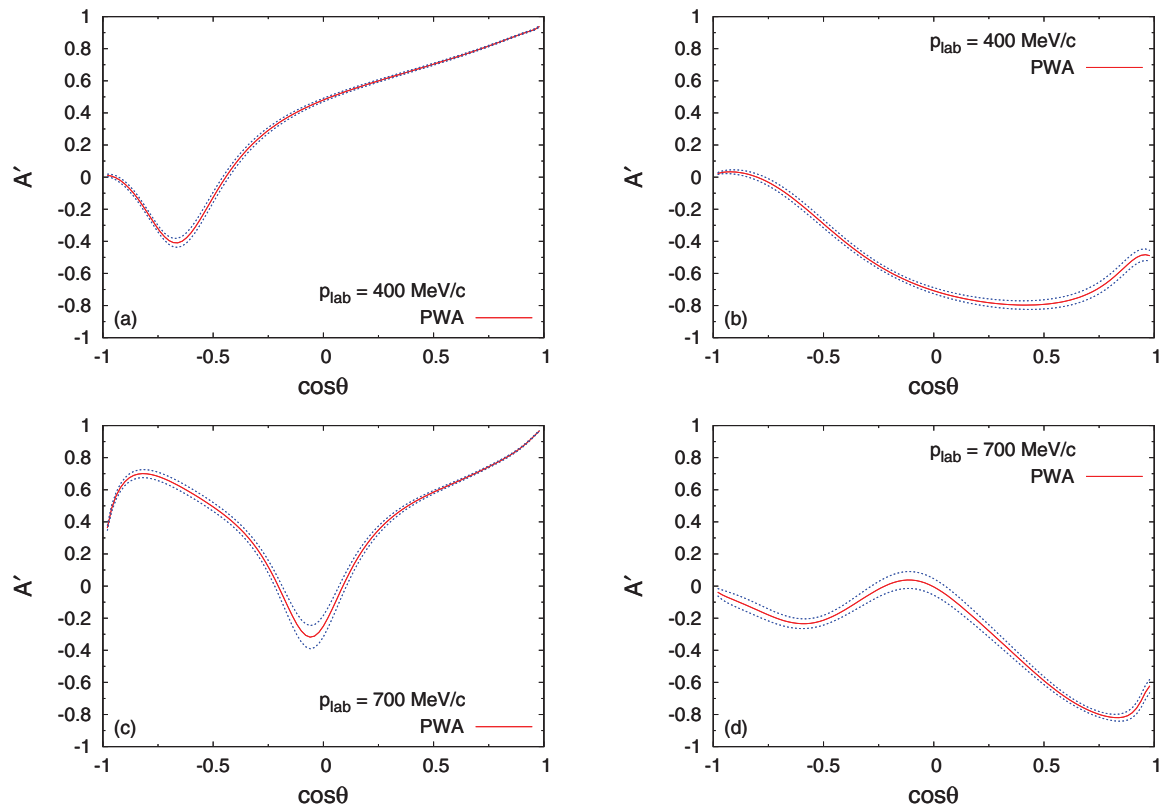

FIG. 7. (Color online) The rotation parameter A for $\bar{p}p$ elastic (left) and charge-exchange (right) scattering at 400 and 700 MeV/c laboratory momentum. The PWA result is given by the solid red line and the dotted blue lines indicate the 1σ uncertainty region.

FIG. 8. (Color online) The rotation parameter A' for $\overline{p}p$ elastic (left) and charge-exchange (right) scattering at 400 and 700 MeV/c laboratory momentum. The PWA result is given by the solid red line and the dotted blue lines indicate the 1σ uncertainty region.
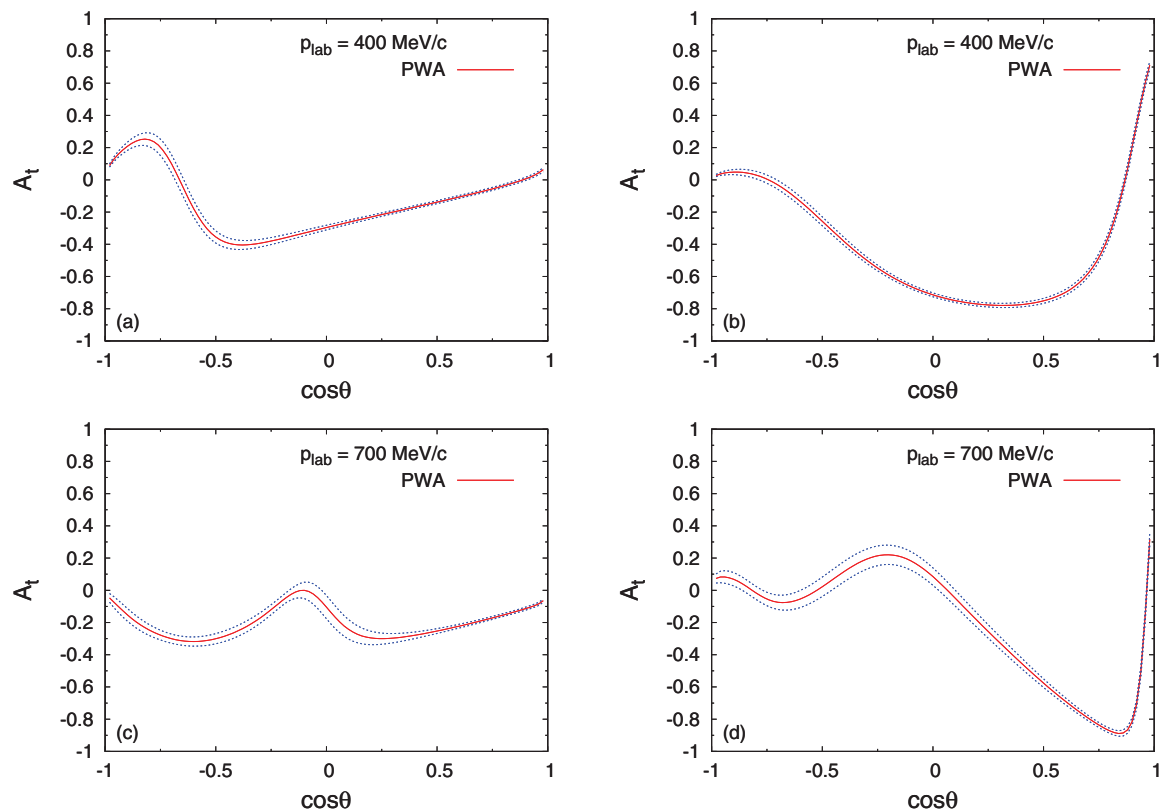

FIG. 9. (Color online) The polarization transfer A_t for $\overline{p}p$ elastic (left) and charge-exchange (right) scattering at 400 and 700 MeV/c laboratory momentum. The PWA result is given by the solid red line and the dotted blue lines indicate the 1σ uncertainty region.
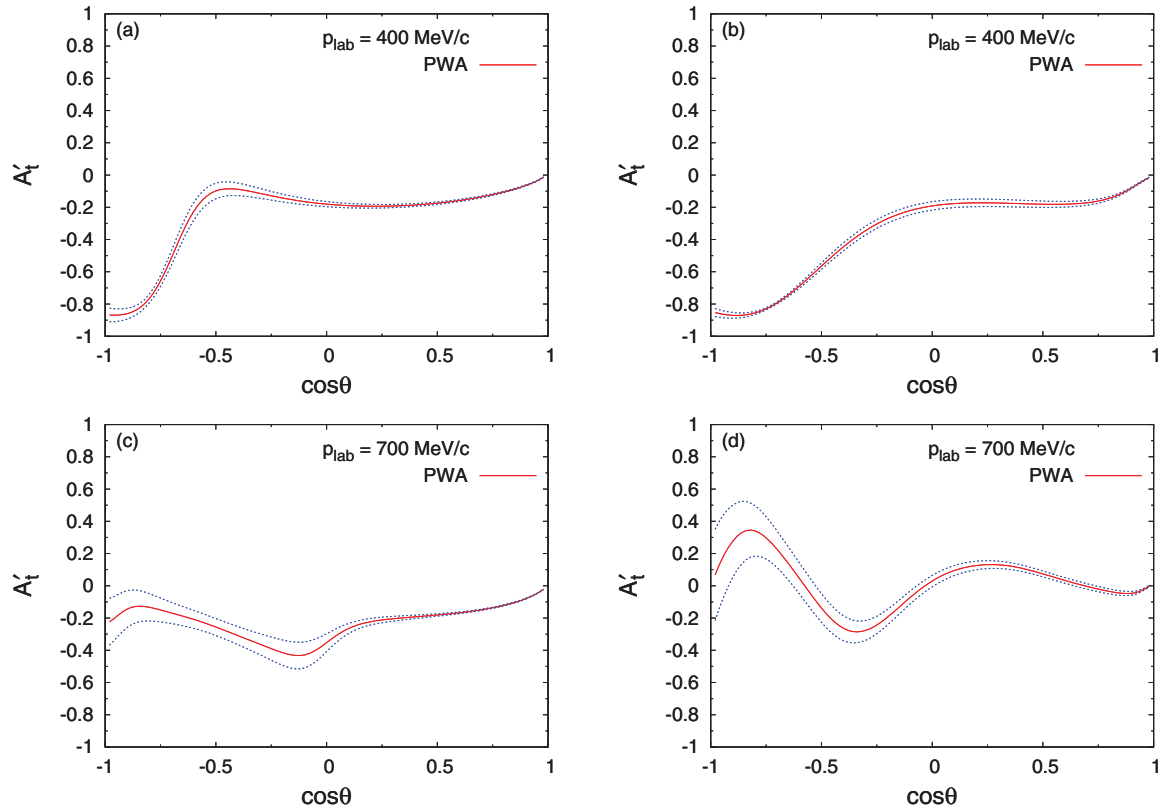
FIG. 10. (Color online) The polarization transfer A_t' for $\bar{p}p$ elastic (left) and charge-exchange (right) scattering at 400 and 700 MeV/c laboratory momentum. The PWA result is given by the solid red line and the dotted blue lines indicate the 1σ uncertainty region.
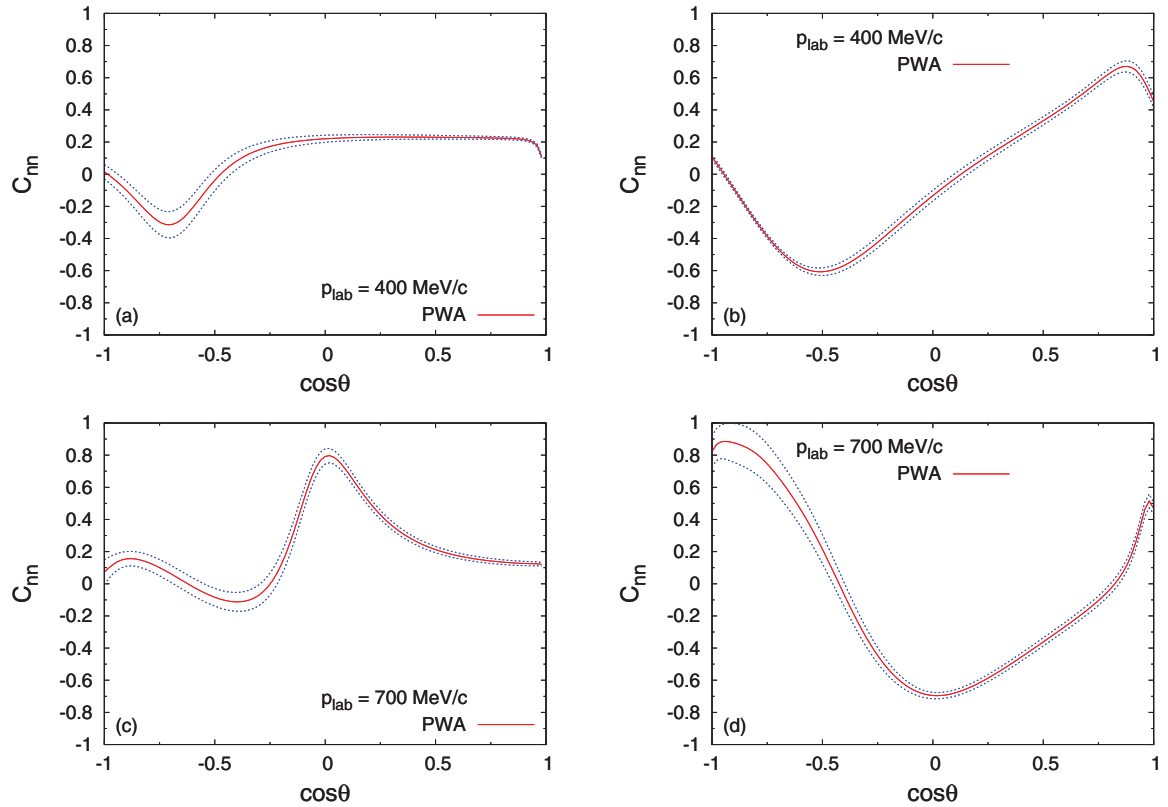

FIG. 11. (Color online) The spin correlation C_{nn} for $\bar{p}p$ elastic (left) and charge-exchange (right) scattering at 400 and 700 MeV/c laboratory momentum. The PWA result is given by the solid red line and the dotted blue lines indicate the 1σ uncertainty region.

FIG. 12. (Color online) The spin correlation A_{zz} for $\overline{p}p$ elastic (left) and charge-exchange (right) scattering at 400 and 700 MeV/c laboratory momentum. The PWA result is given by the solid red line and the dotted blue lines indicate the 1σ uncertainty region.
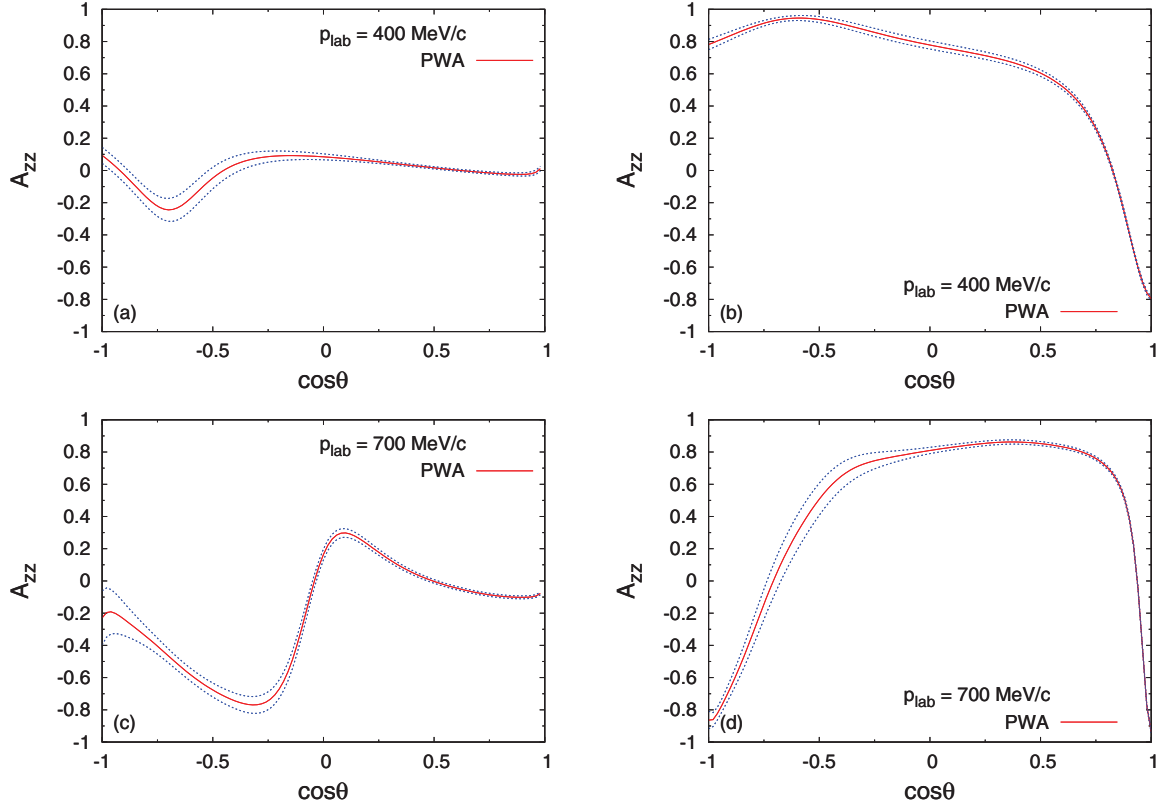
We also study the transverse and longitudinal spin-dependent total cross sections for elastic and charge-exchange scattering. They require a polarized antiproton beam. The spin-dependent cross sections can be written as [35–39,48]

$$\sigma = \sigma_{\text{tot}} - \tfrac{1}{2}\, \boldsymbol{\zeta}_B \cdot \boldsymbol{\zeta}_T\, \Delta\sigma_\perp - \tfrac{1}{2}\, \boldsymbol{\zeta}_B \cdot \hat{\boldsymbol{p}}\, \boldsymbol{\zeta}_T \cdot \hat{\boldsymbol{p}}\, (\Delta\sigma_\parallel - \Delta\sigma_\perp), \tag{8}$$

where $\boldsymbol{\zeta}_B$ and $\boldsymbol{\zeta}_T$ are the unit polarization vectors of the beam and target, respectively, $\hat{\boldsymbol{p}}$ is the unit vector in the direction of the beam momentum, and σ_{tot} is the integrated spin-independent cross section. The differences in the cross sections for antiparallel versus parallel spins, transversely and longitudinally oriented with respect to the beam direction, are

$$\Delta\sigma_\perp = \sigma_{\uparrow\downarrow} - \sigma_{\uparrow\uparrow}, \tag{9a}$$
$$\Delta\sigma_\parallel = \sigma_{\rightleftarrows} - \sigma_{\rightrightarrows}, \tag{9b}$$

where the double arrows mean that the spins of the beam and target particles are antiparallel or parallel, respectively. In terms of $\sigma_{S\mu}$, the integrated cross section with total spin of beam and target particles equal to S with a z component of μ, one has

$$\sigma_{\text{tot}} = \tfrac{1}{2}\sigma_{11} + \tfrac{1}{4}(\sigma_{10} + \sigma_{00}), \tag{10a}$$
$$\Delta\sigma_\perp = -\tfrac{1}{2}(\sigma_{10} - \sigma_{00}), \tag{10b}$$
$$\Delta\sigma_\parallel = -\sigma_{11} + \tfrac{1}{2}(\sigma_{10} + \sigma_{00}). \tag{10c}$$

In Fig. 13 we plot $\Delta\sigma_\perp$ and $\Delta\sigma_\parallel$ for the charge-exchange reaction $\overline{p}p \to \overline{n}n$ for momenta between 100 and 1000 MeV/c. The longitudinal difference $\Delta\sigma_\parallel$ is very large, because of the coherent tensor force from one- and two-pion exchange, and it varies strongly as a function of momentum.
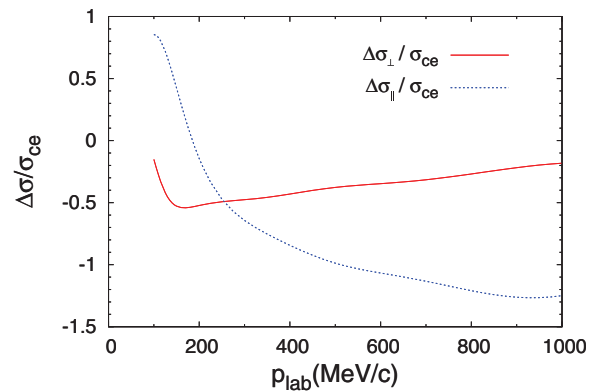

FIG. 13. (Color online) The differences of the transverse and longitudinal cross sections, $\Delta\sigma_\perp$ and $\Delta\sigma_\parallel$, relative to the total cross section σ_{ce} for charge-exchange scattering $\overline{p}p \to \overline{n}n$, as a function of the antiproton laboratory momentum. The solid red line shows the result for the transverse case and the dotted blue line shows the result for the longitudinal case.

III. TOWARD POLARIZED ANTIPROTONS

In this section we investigate the buildup of polarization of a circulating antiproton beam by a polarized proton target. The basic idea is that, since the antiproton-proton total cross section is spin dependent, the number of antiprotons that remain in the beam depends on the spin state of the antiprotons relative to that of the protons. The antiprotons remain in the beam when they are elastically scattered within a certain, very small scattering angle, called the "acceptance angle." These antiprotons can be scattered again in the next revolution of the beam. The antiprotons that interact elastically with larger scattering angle, or undergo charge exchange, or get annihilated are removed from the beam. When the beam is circulated many times in a ring with the target, the remaining beam loses intensity but acquires a net polarization. This mechanism is sometimes called "spin filtering." The feasibility of polarizing a proton beam in this way was demonstrated at the Test Storage Ring in Heidelberg by the experiment FILTEX [49]. Recently, the PAX Collaboration confirmed these results in an experiment at the COSY ring [50]. This raises hope that it could also work experimentally for an antiproton beam.

We follow the methods developed in Refs. [51–56] to calculate the buildup of polarization of an antiproton beam. We present results for antiproton laboratory momenta from 100 to 1000 MeV/c and for typical acceptance angles $\theta_{acc}^{lab} = 5$, 10, 20, and 30 mrad in the laboratory frame. As input we use the scattering amplitudes predicted by our PWA. Our results can be compared to the model calculations of Refs. [53–55]. We assume that the polarization buildup due to the filtering mechanism dominates and that spin-flip mechanisms in the beam can be neglected [52]. This was verified by an experiment in the COSY ring [57].

The scattering amplitude in spin space for a certain momentum and angle is the sum of the electromagnetic and nuclear contributions. Because the filtering mechanism involves forward scattering of a circulating beam, care has to be taken with the treatment of electromagnetic effects [58]. The electromagnetic amplitude, in particular the standard Coulomb scattering amplitude [Eq. (5)], is infinite for $\theta = 0$ (where, in this section, we neglect the small effects of the magnetic-moment interaction). In reality, of course, the Coulomb interaction is screened at very large distances. Since it is not known how to treat this long-range screening, the overall phase of the Coulomb amplitude is unknown. The same holds for the nuclear amplitude, Eq. (7). This implies that electromagnetic effects cannot be separated completely from nuclear effects. The nuclear amplitude contains remnants of the electromagnetic interaction, and one cannot properly define, e.g., the concept of a total hadronic cross section.

The use of a nonzero acceptance angle alleviates the problems associated with extreme forward scattering. Partially integrated elastic and charge-exchange cross sections can be calculated by integrating the differential cross sections for angles $\theta^{lab} > \theta_{acc}^{lab}$. The annihilation amplitude, however, cannot be calculated theoretically. Instead, the annihilation cross section has to be obtained by using the optical theorem for the total $\overline{p}p$ cross section and subtracting the elastic and

charge-exchange cross sections. However, since the optical theorem again involves the forward scattering amplitude, it is strictly not valid for scattering of charged particles [58]. With these caveats in mind, we first review briefly the formalism for the filtering mechanism and then present our results.

Suppose $N_+(t)$ and $N_-(t)$ are the number of antiprotons with spin "up" and spin "down," respectively, at time t; $N_+(0) = N_-(0)$, since the beam is initially unpolarized. The number of antiprotons in the beam as a function of time is given by

$$N(t) = \tfrac{1}{2}N(0)[e^{-\Omega_-^{out}t} + e^{-\Omega_+^{out}t}], \qquad (11)$$

where $\Omega_{\pm}^{out}$ characterize how many antiprotons with spin up or down are scattered out of the acceptance angle [52]. The polarization of the beam is then

$$P_B(t) = \frac{N_+(t) - N_-(t)}{N_+(t) + N_-(t)} = \tanh\left[\frac{t}{2}(\Omega_-^{out} - \Omega_+^{out})\right]. \qquad (12)$$

The relation of $\Omega_{\pm}^{out}$ to the spin-dependent cross sections is given by

$$\Omega_{\pm}^{out} = nf\left\{\sigma_{tot} \mp \tfrac{1}{2}P_T[\Delta\sigma_{\perp} + (\boldsymbol{\zeta}_T \cdot \hat{\boldsymbol{p}})^2(\Delta\sigma_{\parallel} - \Delta\sigma_{\perp})]\right\}, \qquad (13)$$

where n is the areal density of the target, f is the revolution frequency of the beam, and P_T is the polarization of the target. If $|\Omega_-^{out} - \Omega_+^{out}| \ll |\Omega_-^{out} + \Omega_+^{out}|$, as in the case discussed in Refs. [52–54], the beam lifetime is given by

$$\tau_B = \frac{2}{\Omega_-^{out} + \Omega_+^{out}} = \frac{1}{nf\sigma_{tot}}. \qquad (14)$$

One can define a figure of merit by $\mathcal{F}(t) = P_B^2(t)N(t)$, which is maximal at $t = t_0 = 2\tau_B$. The polarizations at t_0 are

$$P_B(t_0) = P_\perp(t_0) = P_T\frac{\Delta\sigma_\perp}{\sigma_{tot}}, \quad \text{when} \quad \boldsymbol{\zeta}_T \cdot \hat{\boldsymbol{p}} = 0, \quad (15a)$$

$$P_B(t_0) = P_\parallel(t_0) = P_T\frac{\Delta\sigma_\parallel}{\sigma_{tot}}, \quad \text{when} \quad \boldsymbol{\zeta}_T \cdot \hat{\boldsymbol{p}} = \pm 1. \quad (15b)$$
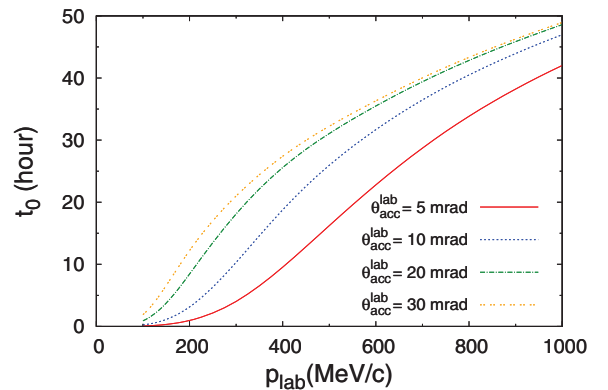

FIG. 14. (Color online) The time t_0 in hours with the areal density of the target, $n = 10^{14}$ cm^{-2}, and the revolution frequency of the beam, $f = 10^6$ s^{-1}, as function of the antiproton beam momentum. The solid red, dotted blue, dot-dashed green, and double-dotted orange lines show the result for acceptance angles $\theta_{acc}^{lab} = 5$, 10, 20, and 30 mrad in the laboratory frame, respectively.

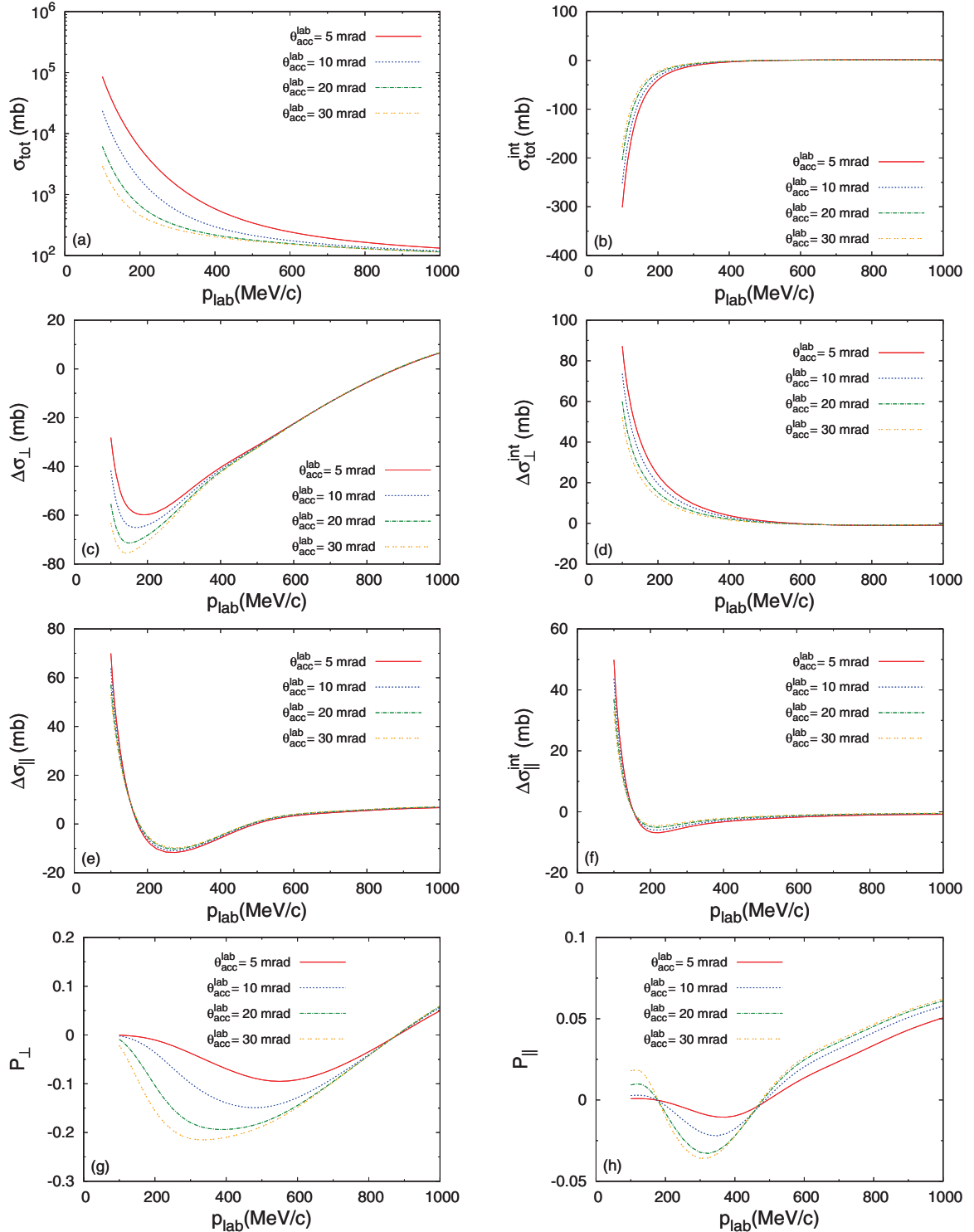FIG. 15. (Color online) The total cross sections σ_{tot}, the interference cross sections $\sigma_{\text{tot}}^{\text{int}}$, the differences of the transverse and longitudinal cross sections, $\Delta\sigma_\perp$ and $\Delta\sigma_\parallel$, and the polarizations $P_\perp$ and $P_\parallel$ at time t_0. The solid red, dotted blue, dot-dashed green, and double-dotted orange lines show the results for $\theta_{\text{acc}}^{\text{lab}} = 5$, 10, 20, and 30 mrad, respectively.

In Fig. 14, the optimal time t_0 as a function of laboratory momentum is plotted for the typical values $n = 10^{14}$ cm^{-2} and $f = 10^6$ s^{-1} and for acceptance angles $\theta_{\text{acc}}^{\text{lab}} = 5$, 10, 20, and 30 mrad in the laboratory frame (with the assumption that

$P_T = 1$). We find that t_0 is of the order of several tens of hours for the momenta and the acceptance angles considered.

In Fig. 15 the integrated cross sections, the integrated Coulomb-nuclear interference cross sections, and the beam

polarizations are given at time t_0 as functions of momentum for the different acceptance angles. The interferences are important for the lower momenta. For a target with polarization perpendicular to the direction of the incoming beam (transverse, $P_B = P_\perp$), the maximal beam polarization is around -15%, depending on the acceptance angle. At momenta around 350 MeV/c, the polarization can reach about -20% for "large" acceptance angle $\theta_{\mathrm{acc}}^{\mathrm{lab}} = 30$ mrad. For "small" acceptance angle $\theta_{\mathrm{acc}}^{\mathrm{lab}} = 5$ mrad, the polarization is about -10% at momenta around 550 MeV/c. When the momentum goes up to 1000 MeV/c, the polarization is around 5%. For a target with polarization collinear with the direction of the incoming beam (longitudinal, $P_B = P_\parallel$), the maximal beam polarization is around -2% at low momenta and 5% at the higher momenta. At low momenta around 300 MeV/c, the polarization reaches about -3% for acceptance angle $\theta_{\mathrm{acc}}^{\mathrm{lab}} = 30$ mrad, while at momenta around 350 MeV/c, the polarization reaches about -1% for acceptance angle $\theta_{\mathrm{acc}}^{\mathrm{lab}} = 5$ mrad. For momenta around 1000 MeV/c, the polarizations are between 5% and 6% when $\theta_{\mathrm{acc}}^{\mathrm{lab}}$ varies between 5 and 30 mrad. In general, the transverse polarization $P_\perp$ reaches higher values than the longitudinal polarization $P_\parallel$. By using the error matrix of the PWA solution, we have estimated that the statistical uncertainty in our predictions for the polarizations $P_\perp$ and $P_\parallel$ is less than 2% in the momentum range considered.

We conclude that, in the momentum range considered here, a significant transverse polarization $P_\perp$ can be achieved within a reasonable time. The signs of the polarizations imply that the beam polarization has the same direction as the target polarization when the sign is positive, while it has the opposite direction when the sign is negative.

IV. SUMMARY AND CONCLUSIONS

Based on our new energy-dependent PWA of all antiproton-proton scattering data below 925 MeV/c, we presented predictions for unmeasured rank-two spin observables, which may be tested by future experiments. Such new spin data can improve the existing solution, provided they are (statistically) precise enough and (systematically) accurate. Since the PWA uses model-independent theoretical input for the long-range electromagnetic and strong interactions and gives an optimal description of the existing database, these predictions are robust and at present the best possible. Striking spin effects are predicted especially for charge-exchange scattering, confirming quantitatively some of the early, pre-LEAR findings of Ref. [33]. These effects are due to the spin dependence of the long-range one- and two-pion exchange interactions, in particular the coherent tensor force, and the spin dependence of the parametrized short-range interaction. In the charge-exchange reaction the values of the polarization-transfer parameters R_t' and A_t are large for the very forward angles at low energies, which suggests a way to produce polarized antineutrons. We investigated the buildup of polarization of a circulating antiproton beam by a polarized proton target as a function of momentum and for several typical acceptance angles. It appears feasible to achieve a significant transverse polarization within a reasonable time. The size of the resulting polarization depends strongly on the momentum of the beam.

[1] S. van der Meer, Rev. Mod. Phys. **57**, 689 (1985).

[2] R. A. Kunne *et al.*, Phys. Lett. B **206**, 557 (1988).

[3] R. A. Kunne *et al.*, Nucl. Phys. B **323**, 1 (1989).

[4] R. Bertini *et al.*, Phys. Lett. B **228**, 531 (1989).

[5] F. Perrot-Kunne *et al.*, Phys. Lett. B **261**, 188 (1991).

[6] R. Birsa *et al.*, Phys. Lett. B **246**, 267 (1990).

[7] R. Birsa *et al.*, Phys. Lett. B **273**, 533 (1991).

[8] R. Birsa *et al.*, Nucl. Phys. B **403**, 25 (1993).

[9] M. Lamanna *et al.*, Nucl. Phys. B **434**, 479 (1995).

[10] R. A. Kunne *et al.*, Phys. Lett. B **261**, 191 (1991).

[11] R. Birsa *et al.*, Phys. Lett. B **302**, 517 (1993).

[12] A. Ahmidouch *et al.*, Nucl. Phys. B **444**, 27 (1995).

[13] A. Ahmidouch *et al.*, Phys. Lett. B **380**, 235 (1996).

[14] P. Lenisa and F. Rathmann (The PAX Collaboration), arXiv:hep-ex/0505054v1.

[15] C. Barschel *et al.* (The PAX Collaboration), arXiv: 0904.2325v1[nucl-ex].

[16] D. Zhou and R. G. E. Timmermans, Phys. Rev. C **86**, 044003 (2012).

[17] J. R. Bergervoet, P. C. van Campen, W. A. van der Sanden, and J. J. de Swart, Phys. Rev. C **38**, 15 (1988).

[18] J. R. Bergervoet, P. C. van Campen, R. A. M. Klomp, J.-L. de Kok, T. A. Rijken, V. G. J. Stoks, and J. J. de Swart, Phys. Rev. C **41**, 1435 (1990).

[19] V. Stoks, R. Timmermans, and J. J. de Swart, Phys. Rev. C **47**, 512 (1993).

[20] V. G. J. Stoks, R. A. M. Klomp, M. C. M. Rentmeester, and J. J. de Swart, Phys. Rev. C **48**, 792 (1993).

[21] M. C. M. Rentmeester, R. G. E. Timmermans, J. L. Friar, and J. J. de Swart, Phys. Rev. Lett. **82**, 4992 (1999).

[22] M. C. M. Rentmeester, R. G. E. Timmermans, and J. J. de Swart, Phys. Rev. C **67**, 044001 (2003).

[23] Nijmegen nucleon-nucleon online service, http://nn-online.org.

[24] J. Carlson and R. Schiavilla, Rev. Mod. Phys **70**, 743 (1998).

[25] H. A. Bethe, Rev. Mod. Phys. **71**, S6 (1999).

[26] R. G. E. Timmermans, Th. A. Rijken, and J. J. de Swart, Phys. Rev. Lett. **67**, 1074 (1991).

[27] R. Timmermans, Th. A. Rijken, and J. J. de Swart, Phys. Rev. C **50**, 48 (1994).

[28] R. Timmermans, Th. A. Rijken, and J. J. de Swart, Phys. Rev. C **52**, 1145 (1995).

[29] R. G. E. Timmermans, T. A. Rijken, and J. J. de Swart, Nucl. Phys. A **479**, 383 (1988).

[30] J. J. de Swart, T. A. Rijken, P. M. Maessen, and R. Timmermans, Il Nuovo Cimento **102A**, 203 (1989).

[31] R. G. E. Timmermans, Th. A. Rijken, and J. J. de Swart, Phys. Lett. B **257**, 227 (1991).

[32] R. G. E. Timmermans, Th. A. Rijken, and J. J. de Swart, Phys. Rev. D **45**, 2288 (1992).

[33] C. B. Dover and J.-M. Richard, Phys. Rev. C **25**, 1952 (1982).

[34] L. Wolfenstein and J. Ashkin, Phys. Rev. **85**, 947 (1952).

[35] N. Hoshizaki, Prog. Theor. Phys. Suppl. **42**, 107 (1968).

[36] J. Bystricky, F. Lehar, and P. Winternitz, J. Phys. France **39**, 1 (1978).

[37] P. LaFrance and P. Winternitz, J. Phys. France **41**, 1391 (1980).

[38] J. Bystricky, F. Lehar, and P. Winternitz, J. Phys. France **45**, 207 (1984).

[39] P. LaFrance, F. Lehar, B. Loiseau, and P. Winternitz, Helv. Phys. Acta **65**, 611 (1992).

[40] R. A. Kunne, in *Medium-Energy Antiprotons and the Quark-Gluon Structure of Hadrons*, *Proceedings of the International School of Physics with Low-Energy Antiprotons* (International School of Nuclear Physics, Erice, Italy, 1990), edited by R. Landau, J.-M. Richard, and R. Klapisch (Plenum Press, N.Y., 1992); preprint LNS/Ph/90-18.

[41] L. Puzikov, R. Ryndin, and J. Smorodindky, Nucl. Phys. **3**, 436 (1957); C. R. Schumacher and H. A. Bethe, Phys. Rev. **121**, 1534 (1961).

[42] J.-M. Richard, Phys. Rev. C **52**, 1143 (1995).

[43] A. Martin *et al.*, Nucl. Phys. A **487**, 563 (1988).

[44] L. Durand and J. Sandweiss, Phys. Rev. **135**, B540 (1964).

[45] K. D. Paschke and B. Quinn, Phys. Lett. B **495**, 49 (2000).

[46] B. Bassalleck *et al.*, Phys. Rev. Lett. **89**, 212302 (2002).

[47] K. D. Paschke *et al.*, Phys. Rev. C **74**, 015206 (2006).

[48] S. M. Bilenky and R. M. Ryndin, Phys. Lett. **6**, 217 (1963).

[49] F. Rathmann *et al.*, Phys. Rev. Lett. **71**, 1379 (1993).

[50] W. Augustyniak *et al.*, Phys. Lett. B **718**, 64 (2012).

[51] P. L. Csonka, Nucl. Instrum. Methods **63**, 247 (1968).

[52] A. I. Milstein and V. M. Strakhovenko, Phys. Rev. E **72**, 066503 (2005).

[53] V. F. Dmitriev, A. I. Milstein, and V. M. Strakhovenko, Nucl. Instrum. Methods B **266**, 1122 (2008).

[54] V. F. Dmitriev, A. I. Milstein, and S. G. Salnikov, Phys. Lett. B **690**, 427 (2010).

[55] J. Haidenbauer, J. Phys. Conf. Ser. **295**, 012094 (2011).

[56] Yu. N. Uzikov and J. Haidenbauer, J. Phys. Conf. Ser. **295**, 012087 (2011).

[57] D. Oellers *et al.*, Phys. Lett. B **674**, 269 (2009).

[58] J. J. de Swart, M. C. M. Rentmeester, and R. G. E. Timmermans, Pion-Nucleon Newsl. **13**, 96 (1997).